IEEE Open Journal of
Power Electronics

Received 13 March 2020; revised 5 May 2020; accepted 10 May 2020. Date of publication 5 June 2020; date of current version 18 June 2020. The review of this article was arranged by Associate Editor Prof. Xiong Du.

Digital Object Identifier 10.1109/OJPEL.2020.3000466

Hysteresis Model Predictive Current Control for PMSM With LC Filter Considering Different Error Shapes

STEFAN WALZ (Student Member, IEEE), AND MARCO LISERRE (Fellow, IEEE)

Chair of Power Electronics, Kiel University, 24118 Kiel, Germany

CORRESPONDING AUTHOR: STEFAN WALZ (e-mail: swa@tf.uni-kiel.de)

This work was supported by the European Union/Interreg V-A - Germany-Denmark, under the PE:Region Project.

ABSTRACT This paper investigates three-phase two-level VSI hysteresis-based Model Predictive Control (MPC) for permanent magnet synchronous machines with different current error shapes. To limit the motor current harmonics and prevent overheating of the magnets, motor filters (mostly LC filters) are often used. The hysteresis-based MPC is investigated to provide high dynamic performance and limit the size of the filter. To compensate the resonance introduced by the LC filter and to improve system efficiency, a virtual resistor active damping strategy is implemented. To avoid additional sensors, the filter states are determined by a Luenberger Observer. However, up to now these strategies have never been investigated together with MPC and different current error shapes for motor applications. Simulation results for the different strategies prove the performance efficiency and experimental tests verify the results in a laboratory environment.

INDEX TERMS Current control, permanent magnet motors, predictive control, LC filter, variable speed drives.

I. INTRODUCTION

For electrical drive applications, the field-oriented control (FOC) with a cascaded speed and current regulator is used in industry since many years. The permanent magnet synchronous machine is the first choice for many applications and due to the compact size, high power density and good efficiency permanent magnet machines are widely used in industry [1]. At low ratios of switching frequency to electrical frequency (f_{sw}/f_{el}) the linear control gets instable. For high-speed drives, the rated electrical frequency of the machine can reach very high values [2]. Nevertheless, for medium to high power drives, the switching frequency f_{sw} has to be kept low [3], [4]. In case the natural filtering due to the machine inductances is not sufficient, the low pulse ratio results in high current and voltage harmonics and can heat up the permanent magnets of the machine. To prevent overheating and irreversible demagnetization, a filter may be used to reduce the accruing harmonics [5].

Model predictive control offers the possibility to reduce the effective switching frequency of the converter while maintaining fast dynamic response, and good steady-state performance, while the losses are evaluated and minimized, which is important assuming a cascaded control structure [6], [7]. Moreover, deadbeat predictive control can be used to null the control error after a predefined number of switching periods and obtains very good dynamic performance [8]. It can easily applied be to three or more level converters [9], but is weak under parameter mismatch and requires a modulator [10].

Compared to pulse width modulation (PWM) based control algorithms, MPC needs no modulator. One popular strategy is the Finite Control Set (FCS) MPC, for example shown in [11]. The cost function can be used to optimize performance, losses, or other objectives, but can raise high computational requirements compared to standard PI-based control. At each sampling instant, based on the discrete mathematical model of the system, the control period is used to calculate all possible future states. In [12] modulation and predictive current control for low switching frequencies are shown.

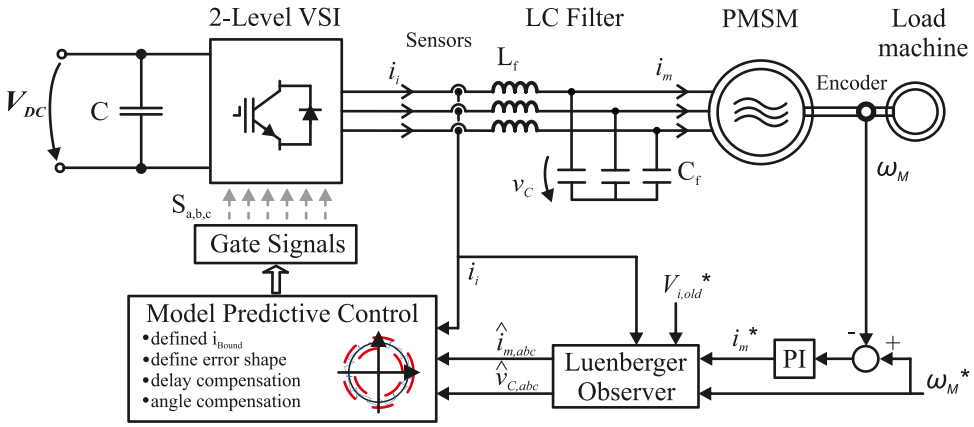

FIGURE 1. Schematic of electrical system with Model Predictive Control.

In [13] a comparison of MPC schemes is given for medium voltage induction machines. The robustness can be improved using flexible control Lyapunov function or disturbance observer [14], [15]. In [16] an overview on hysteresis based MPC or also called model predictive direct current control with different current bounds and switching horizons is presented, while in [17] a direct model predictive control scheme with multiple prediction steps is proposed. This increases the computational effort significantly. In general, one-step MPC algorithm is not critical, and with the ongoing development of modern digital signal processors (DSPs), more advanced algorithms and more system states are becoming possible, e.g. [18] investigates a hysteresis MPC strategy for VSI with LCL filter and constant switching frequency. The virtual resistor (VR) based active damping for medium voltage grid-connected LCL filters is shown in [19]. In [20], [21] active damping strategies for grid-connected VSC with LCL with FCS-MPC and measured states are presented. For a motor output filter, in [22] an observer based PWM strategy is shown and [23] shows VSC direct torque control for MV induction motors with LC filter.

In this paper the effective combination of model predictive control for a PMSM with LC filter in combination with an observer based virtual resistor active damping strategy is proven for the first time. Different hysteresis current error shapes are analyzed and all results are compared with PWM based direct-designed PI Control.

The paper is organized into five sections. First, an overview about the investigated system is given in Section II. In Section III, the model predictive direct current control is analyzed. The LC filter with the Luenberger Observer and the active damping scheme are investigated in Section IV. Section V gives a simulation based comparison, the simulation results of the evaluated control schemes are verified by experiments in Section VI. Conclusions are finally drawn in Section VII.

II. ELECTRICAL SYSTEM MODEL

A 2-level VSI is used to control the motor, the schematic of the system is given in Fig. 1. Different to PI based structures with PWM, the MPC is directly calculating the duty cycles to control the IGBTs of the VSI. The processing and calculation period takes one sampling period. In (1) and (2), the motor equations for a digital control without consideration of the LC filter are given. The voltages are calculated based on the predicted currents and the output voltages based on the sampled values and are applied at the (k+2)-th period. The measured values in the k-th period are used for the calculations of the (k+1)-th period and $i^*_{dq}(k)$ are used as reference currents. Throughout this paper normalized per unit (p.u.) values will be used. As the motor control is in rotating dq-reference frame, all three-phase system variables $x_{a,b,c}$ are transformed to the rotor flux oriented frame with the rotational speed $\omega_{el} = 2\pi \cdot f$.

$$v_d(k+1) = \frac{L_d}{T_S}\left(i^*_d(k) - i_d(k+1)\right) + R_s i_d(k+1) - L_q \omega_{el} i_q(k+1) \quad (1)$$

$$v_q(k+1) = \frac{L_q}{T_S}\left(i^*_q(k) - i_q(k+1)\right) + R_s i_q(k+1) + L_d \omega_{el} i_d(k+1) + \omega_{el}\Psi_{PM} \quad (2)$$

The hysteresis based MPC algorithms are compared with a discrete-time current regulator, e.g. shown in [24]. Using the Euler Method to discretize a continuous time PI Controller is not sufficient for increasing ratios of electrical to switching frequency. In Fig. 2, the Pole-Zero-Map of the discretized PI Control and discrete-time direct designed PI Control are compared. At a frequency of $f_{el}/f_S \approx 14$, the poles drift out of the unit circle and the control gets unstable. The direct design in the discrete time domain uses pole-zero cancellation and helps to overcome this frequency dependent instability.

The maximum sinusoidal voltage that can be provided by SVM considering overmodulation is $|V^*_{sin,max}| = \frac{1}{\sqrt{3}} V_{DC}$. In block operation, the maximum voltage is defined by the absolute value of the space vectors, $|V^*_{block,max}| = |V_{vector}| = \frac{2}{3} V_{DC}$. If the reference voltage is bigger than $|V^*_{sin,max}|$, but still inside the hexagon defined by the space vectors, the applied voltages and currents will contain increased harmonic content. Using model predictive control at high modulation factors, it

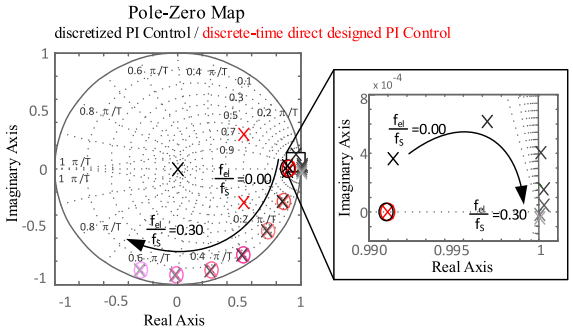

FIGURE 2. Pole-Zero map of Discretized PI Control (black) and discrete-time direct designed PI Control (red) for $f_{el}/f_S = [0.00, 0.05, \ldots, 0.30]$.

has to be made sure, that the reference voltage is actually in the voltage hexagon.

III. HYSTERESIS BASED MODEL PREDICTIVE CONTROL

The hysteresis-based MPC (or direct MPC/ MPC with bounds) uses the motor equations to predict current trajectories of future switching states. The bounds define the current trajectory and the cost function chooses the voltage vector that guarantees to keep the current inside the bounds for the longest period, while minimizing the switching instances. By choosing the bound size, the THDi of the current can be influenced. One main advantage of using hysteresis-based MPC is the long prediction horizon [13]. For one prediction step, the optimization is for example shown in [25]. Additionally, parameter mismatches due to converter non-linearities, dead-times, or saturation have to be taken into account. Considering a decreasing ratio of electrical to switching frequency $f_{el}/f_{sw,eff}$, it is also very important, that the angular displacement is compensated. Especially for long prediction horizons, the angle changes significantly.

For the three-phase two level VSI 2^3 different switch positions are defined. $S_i = 1$ ($i \in \{a, b, c\}$) means the upper device of phase i is closed and the positive electric potential $+V_{DC}$ is applied, while the lower device has to be opened. $S_i = 0$ defines the active lower half bridge and the phase output voltage is 0.

The current at the end of the sampling period can be predicted accurate by using the motor equations (1) and (2) and dissolve after $i_{dq,pred} = i_{dq}(k+1)$. Based on all possible voltage vectors, the current trajectories can be predicted. The redundant zero vectors can be calculated once and optimized later based on the previous voltage vector.

$$i_d^i(k+2) = i_d(k+1) + \frac{T_S}{L_d}\left(v_d^i(k+1) - R_s i_d(k+1) + \omega_{el} L_q i_q(k+1)\right) \tag{3}$$

$$i_q^i(k+2) = i_q(k+1) + \frac{T_S}{L_q}\left(v_q^i(k+1) - R_s i_q(k+1) - \omega_{el} L_d i_d(k+1) - \omega_{el}\Psi_{PM}\right) \tag{4}$$

A. CIRCULAR CURRENT ERROR SHAPE

A circular current error bound is an easy to check criteria for the hysteresis based MPC. Based on the amplitude and angle change of the current, the trajectories T_x^i for the different switching states can be predicted as shown for example in [25], while i_{Bound} can be used to regulate the THDi. These trajectory calculations are done every control period. By comparing the current error at the end of every control period ($i_{dq,pred}$) with the defined current boundary, it can be guaranteed, that the current stays always inside the bounds. If the current error is bigger than the bound, a new index respectively voltage vector is chosen by maximizing the cost function (5), taking into account the number of commutations n_{com} needed to apply the new voltage vector.

$$ind = \max_{i\in[1\ldots7]}\left(\frac{n_i}{n_{\text{com}}}\right) \tag{5}$$

Even though the results can be fraction numbers, this term gives an idea of how many sampling periods per commutation the current will stay inside the bounds. For example, it is preferable to choose a voltage vector that keeps the current inside the bounds for three sampling periods with only one switching operation, instead of a voltage vector that provides five sampling periods but needs two commutations.

Problems can occur, when two vectors provide the same number of periods. To prevent that in this case always the same solution is chosen, the cost function is extended by a correction term c_i. If two or more solutions provide the same number of periods, the solution with the smaller mean error should be chosen. Hence, the accumulated error $e_{i,\text{accum}}$ is divided by the predicted number of periods n_p^i and added to the cost function (5). This ensures the best initial position for the next optimization period.

$$c_i(k) = \frac{\sum ||i_{dq}^*(k) - i_{dq}^i(k+T_n)||}{i_{\text{Bound}} \cdot n_p^i} \tag{6}$$

B. RECTANGULAR CURRENT ERROR SHAPE

Current error limits in the shape of a square are an easy to program alternative. The limits for the maximum d-/ and q-errors can be defined separately, resulting in a rectangular shape. In this way, the maximum flux distortion can be defined by the d-current error and the torque distortion by defining the maximum q-current error. A major drawback of this method is the maximum allowed absolute current error. As d-/ and q-current error are defined separately, the maximum current error is $\sqrt{2}$ times the defined limits. This has to be taken into account designing the converter and the component layout.

C. HEXAGONAL CURRENT ERROR SHAPE

Based on the motor equations (1) and (2), the current trajectories for the hexagonal current error shape can be calculated gradually until the trajectory gets out of the bounds. For each trajectory the number of sampling periods is calculated in which the current stays inside its limits $n_{i,i\in[1\ldots7]}$. The number of commutations to reach this switching states is used to

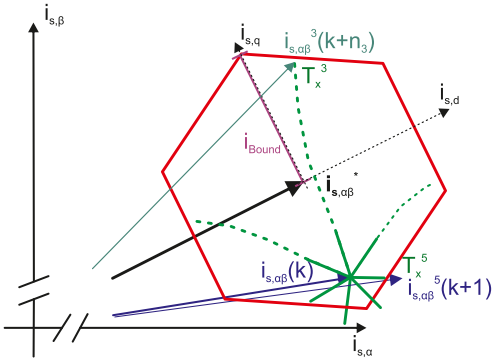

FIGURE 3. Alpha-beta current trajectories for hexagonal error shape.

optimize the cost function. Equation (6) can be used in case two voltage vectors provide the same number of periods. Even though this method is more complex, it is shown in [16] that these bounds are based on the natural bounds of each stator phase current.

Exemplary current trajectories in the α-β / d-q reference frame are shown in Fig. 3. The reference current vector $i^*_{s,\alpha\beta}$ is depicted in black. The sampled current at the recent time step (k) $i_{s,\alpha\beta}(k)$ is shown in blue. It is detected, that the current $i_{s,\alpha\beta}(k+1)$ will be out of the bounds in the next period. Hence, all possible current trajectories have to be calculated. The seven different current trajectories for a 2-Level Converter are shown in green. Depending on the number of commutations and the number of periods in which the trajectory remains within the hexagon, the voltage vector is selected.

IV. CONTROL IN CASE OF LC FILTER

In Section V, it is shown that the current distortion (THDi) is very high for low switching frequencies. A typical way to reduce the THDi is the use of motor filters, such as sine wave / LC filters. The inverter output voltage v_i is filtered and the motor is supplied with smoothed currents i_m. With the added filter inductance and capacitor, a second order system is added to the system, resulting in a more complex control of the PMSM.

The mathematical model of the LC filter is given in (7) and (8), the resonance/cut-off frequency can be calculated according to (9).

$$\frac{\mathrm{d}i_{i,d}}{\mathrm{d}t} = \frac{1}{L_f}v_{i,d} - \frac{1}{L_f}v_{C,d} + \omega_{el}i_{i,q} \tag{7}$$

$$\frac{\mathrm{d}i_{i,q}}{\mathrm{d}t} = \frac{1}{L_f}v_{i,q} - \frac{1}{L_f}v_{C,q} - \omega_{el}i_{i,d} \tag{8}$$

$$f_{\mathrm{res}} = \frac{1}{2\pi}\frac{1}{\sqrt{L_f C_f}} \tag{9}$$

A. CONTINUOUS TIME MODEL

The continuous time state space representation of the LC filter and PMSM in the d/q reference frame is given in (10). The state vector is $\underline{x} = [i_{i,d}\ \ i_{i,q}\ \ v_{C,d}\ \ v_{C,q}\ \ i_{m,d}\ \ i_{m,q}]^T$,

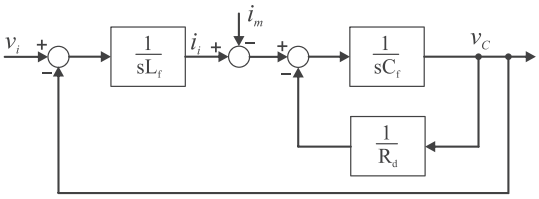

FIGURE 4. s-domain block diagram of LC filter with virtual damping resistor.

where $i_{i,d}$, $i_{i,q}$, $v_{C,d}$, $v_{C,q}$, and $i_{m,d}$, $i_{m,q}$ are the direct and quadrature components of the inverter current, filter capacitor voltage, and the motor current. The internal resistances of the filter inductor and filter capacitor are neglected.

$$\frac{dx(t)}{dt} = \boldsymbol{A}_m\boldsymbol{x}(t) + \boldsymbol{B}_m\boldsymbol{v}_i(t) + \boldsymbol{B}_{m1} \tag{10}$$

$$\boldsymbol{A}_m = \begin{bmatrix} 0 & \omega_{el} & -\frac{1}{L_f} & 0 & 0 & 0 \\ -\omega_{el} & 0 & 0 & -\frac{1}{L_f} & 0 & 0 \\ \frac{1}{C_f} & 0 & 0 & \omega_{el} & -\frac{1}{C_f} & 0 \\ 0 & \frac{1}{C_f} & -\omega_{el} & 0 & 0 & -\frac{1}{C_f} \\ 0 & 0 & \frac{1}{L_d} & 0 & -\frac{R_s}{L_d} & \omega_{el} \\ 0 & 0 & 0 & \frac{1}{L_q} & -\omega_{el} & -\frac{R_s}{L_q} \end{bmatrix}$$

$$\boldsymbol{B}_m = \begin{bmatrix} \frac{1}{L_f} & 0 \\ 0 & \frac{1}{L_f} \\ 0 & 0 \\ 0 & 0 \\ 0 & 0 \\ 0 & 0 \end{bmatrix}, \quad \boldsymbol{B}_{m1} = \begin{bmatrix} 0 \\ 0 \\ 0 \\ 0 \\ 0 \\ -\frac{\Psi_{\mathrm{PM}}\omega_{el}}{L_q} \end{bmatrix}$$

B. DISCRETE TIME MODEL

For the implementation in a digital control, the continuous time model has to be discretized by calculating the matrix exponential $e^{A_m T_S}$ using the Euler method and approximating the error, with I_{6x6} denoting an 6 x 6 identity matrix [20].

$$x(k+1) = e^{A_m T_S}x(k) \tag{11}$$

$$\boldsymbol{F}_m = e^{A_m T_S} \approx I_{6x6} + \frac{\boldsymbol{A}_m T_S}{1!} + \underbrace{\frac{(\boldsymbol{A}_m T_S)^2}{2!} + \ldots}_{\approx 0} \tag{12}$$

$$\begin{aligned} \boldsymbol{G}_m &= \boldsymbol{A}_m^{-1}(\boldsymbol{F}_m - I_{6x6})\boldsymbol{B}_m \\ \boldsymbol{G}_{m1} &= \boldsymbol{A}_m^{-1}(\boldsymbol{F}_m - I_{6x6})\boldsymbol{B}_{m1} \end{aligned} \tag{13}$$

With equations (10)-(13), the complete discrete time state space representation is given and can be used for the model predictive controller and the Luenberger Observer.

C. HMPC FOR PMSM WITH LC FILTER

The transfer function of the LC filter is given in (14), the frequency domain representation is shown in Fig. 4 as well as

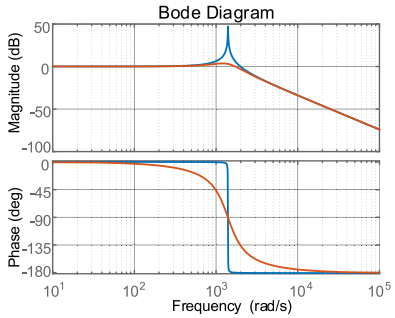

FIGURE 5. Bode plot of LC filter transfer function with $Q = \frac{2}{\sqrt{2}}$ (red) and without damping resistance (blue).

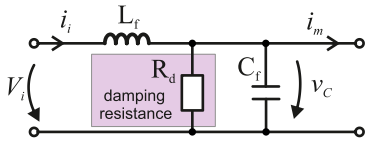

FIGURE 6. Single phase diagram of virtual resistor damped LC filter.

the Bode plot for a damping ratio of quality factor of $Q = \frac{1}{\sqrt{2}}$ (red) and without damping resistance (blue), Fig. 5.

$$P_{LC}(s) = \frac{v_C}{v_i} = \frac{1}{sL_f\left(sC_f + \frac{1}{R_d}\right)} \tag{14}$$

By adding the LC filter, the applied voltage vectors no longer have a direct effect on the motor dynamics. An effective and simple way to overcome this issue is to introduce new control variables. The reference motor currents obtained by the speed controller can be transformed to reference inverter currents, taking into account the filter capacitor currents [21].

$$i^*_{i,d}(k) = i^*_{m,d}(k) - \omega_{el}C_f v_{C,q}(k) \tag{15}$$

$$i^*_{i,q}(k) = i^*_{m,q}(k) + \omega_{el}C_f v_{C,d}(k) \tag{16}$$

D. VIRTUAL RESISTOR (VR) BASED ACTIVE DAMPING

To damp the resonance of the LC filter, a virtual resistor based active damping scheme is chosen and included in the HMPC. This way, no additional hardware has to be added and the efficiency is not corrupted. In [19] different VR based strategies to achieve resonance damping are shown. A virtual resistor R_d in parallel to the filter capacitor is chosen to avoid numerical differentiation, Fig. 6.

The virtual resistor current can be derived from the frequency domain analysis, eq. (17), and then be converted to the time domain. Based on the capacitor voltage ripple, which can be derived by a high pass filter, a current reference i^*_{Rd} can be calculated as shown in eq. (18) [19].

$$i^*_{Rd}(s) = -\frac{v_C(s)}{R_d} \tag{17}$$

$$i^*_{Rd}(k) = -\frac{v_C(k)}{R_d} \tag{18}$$

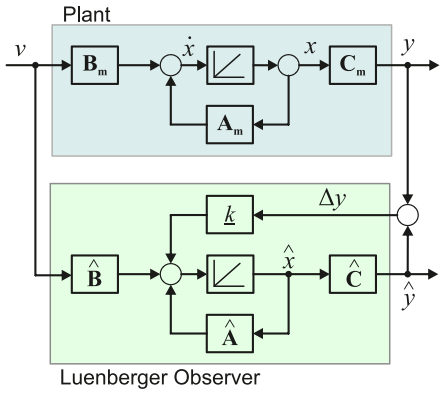

FIGURE 7. Schematic of Luenberger Observer.

Hence, the overall inverter current reference for the PMSM with LC filter and VR based active damping can be approximated by

$$i^*_{i,d}(k) = i^*_{m,d}(k) - \omega_{el}C_f v_{C,q}(k) - \frac{v_{C,d}(k)}{R_d} \tag{19}$$

$$i^*_{i,q}(k) = i^*_{m,q}(k) + \omega_{el}C_f v_{C,d}(k) - \frac{v_{C,q}(k)}{R_d} \tag{20}$$

E. LUENBERGER OBSERVER

A straightforward way to control a PMSM with LC filter is to additionally measure the capacitor voltage v_C and the motor currents i_m. However, these sensors would increase the system cost, reduce the reliability if they fail, or it is just not possible to mount and connect additional sensors due to limited space conditions. To reduce the number of sensors, here a Luenberger Observer is used. Generally, for most industry applications, the inverter side currents are measured for security reasons. Thus, using the feedback of these currents for the Luenberger Observer is a promising approach to implement the observer.

The Luenberger Observer is based on a copy of the plant with an additional error feedback $\underline{k}$. The schematic of the observer is shown in Fig. 7. The observer based states are marked by the superscript symbol'^'.

The observability of the system can be proven by investigating the observability matrix $\underline{M}_0$. The inverter side current is used as state feedback, defining $\boldsymbol{C}$ as

$$\boldsymbol{C} = [1\ \ 1\ \ 0\ \ 0\ \ 0\ \ 0]^T \tag{21}$$

Hence, the observability matrix becomes eq. (17) and the rank of $\underline{\boldsymbol{M}}_0$ is equal to the number of states for realistic parameter and $\omega > 0$ and the system is therefore observable [26].

$$\underline{\boldsymbol{M}}_0 = \left[\boldsymbol{C}\ \ \boldsymbol{CA_m}\ \ \boldsymbol{CA_m}^2\ \ \boldsymbol{CA_m}^3\ \ \boldsymbol{CA_m}^4\ \ \boldsymbol{CA_m}^5\right]^T \tag{22}$$

The choice of the observer gain vector $\underline{k}$ is a tradeoff between fast transient response and sensitivity to parameter mismatches and interference noise. Typically a program like

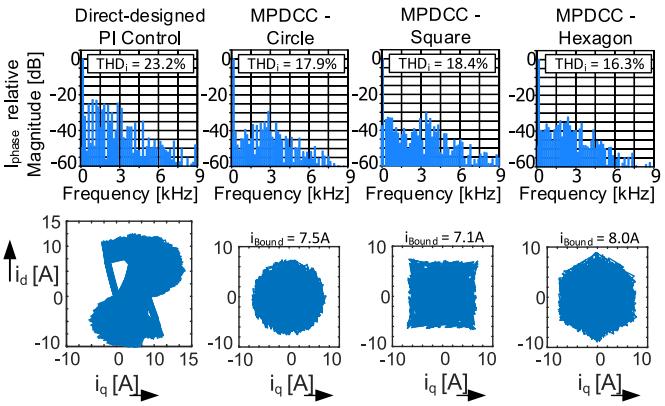

FIGURE 8. Relative Magnitude of VSI phase current (without LC filter) $i_{i,a}$ in dB and $i_{m,dq}$ error circle for eff. switching frequency of $f_{sw,eff} = 1500$ Hz.

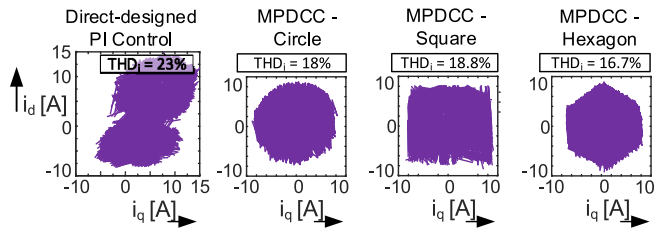

FIGURE 9. Laboratory measurements for VSI (without LC filter) $i_{m,dq}$ current error circle for eff. switching frequency of $f_{sw,eff} = 1500$ Hz.

Matlab and the 'place' function can be used and the poles can be placed similar to the controller design to achieve the desired dynamics. In [22] a comparison of pole placement and a constant gain is given, showing good dynamic and steady state performance can be achieved by a simple observer gain vector $\underline{k} = [k_1 \;\; k_2 \;\; 0 \;\; 0 \;\; 0 \;\; 0]^T$. With k_1, k_2 approximately determining the bandwidth of the estimator, a fast and sufficient tuning for this application is chosen.

V. SIMULATION RESULTS

In Fig. 8 simulation results of the relative magnitude of the phase current for the two level VSI without motor filter are compared, proving the applicability of the different current error shapes. While the operation point of 50 Hz is challenging for PI Control, the peak around the 1500 Hz sidebands can be seen. For the MPC strategies, the THDi is smaller and no regular pattern can be seen. From the dq-error current circle, square, and hexagon it can be seen, that the MPC requires a current bound of 7.5A, 7.1A, and 8.0A and stays perfectly inside the bounds, while the PI Control has bigger current variations.

Figure 12 (dotted lines) show the simulation results for the important operation point at nominal frequency. It can be seen, that the hysteresis-based MPC is preferable at all points. Comparing for example the THDi of 25%, by using hysteresis-based MPC the effective switching frequency can be reduced by over 25%, from $f_{sw,eff} = 1260$ Hz to 830 Hz. In addition, the advantages of using the hexagonal error shape

TABLE I Converter Setup Data

V_{DC}	560V
$f_S = f_{\mathrm{control}}$	10kHz
T_{deadtime}	1.5μs

TABLE II Machine Setup Data

$P_{\mathrm{PMSM,nom}}$	15kW
I_{max}	35A
f_{rated}	50Hz
$L_{\mathrm{s,dq}}$	3.0mH
R_{s}	0.08Ω

TABLE III Sinewave Filter Data

L_{f}	3.0mH
C_{f}	100μF

can be seen, the effective switching frequency can be reduced by 5%-10%, compared to the circular and square error bound. For the challenging operating area of $f_{sw}/f_{el} < 20$ the advantages of the model predictive strategies is most significant.

The simulation results with the LC filter and the observer based control with active damping are shown in Figure 14, dotted lines. By adding the Filter, the current distortion is improved significantly, especially for the direct designed PI Control. Due to the regular switching pattern of the PWM based control, the filter can attenuate the harmonics very successfully. The model predictive based algorithms have variable switching frequency, which results in uneven distribution of the harmonics. For decreasing pulse ratios, the MPC strategies get more advantageous and are providing better THDi for pulse ratios $f_{sw}/f_{el} < 16$.

VI. EXPERIMENTAL RESULTS

The simulation results of the controllers are validated by experiments with a 15kW *Siemens PMSM*, connected to a DC load machine. The motor filter is a sinewave filter by Danfoss Drives with adjusted capacitors. The ratio of electrical to switching frequency f_{el}/f_{sw} is equivalent to e.g. a high-speed machine or slow switching high power drives. The DC link of the converter is connected to a 20kW DC voltage source. The waveform of the output current is measured and recorded by a *Tektronix DPO3014 Oscilloscope* with a *Tektronix TCP0030* Current Probe and a *dSPACE MicroLabBox 1202* with *ControlDesk*. The current distortion is measured with the *YOKOGAWA WT3000E* precision power analyzer. The inductance and resistance of the machine, as well as the sinewave filter parameters were measured with a *Sourcetronic ST2826A LCR meter* and are given in Table II and Table III. The *dSPACE MicroLabBox* is used to control the system.

In Fig. 9 (purple), the different current error shapes at nominal frequency and an effective switching frequency of $f_{sw(,eff)} = 1500$ Hz shown. Compared to the simulation results in Fig. 8 (blue), it can beseen that the results are very similar. For the model predictive schemes, the bounds are increased slightly. In the laboratory environment with uncertainties such as line inductances, motor saturation and saliency,

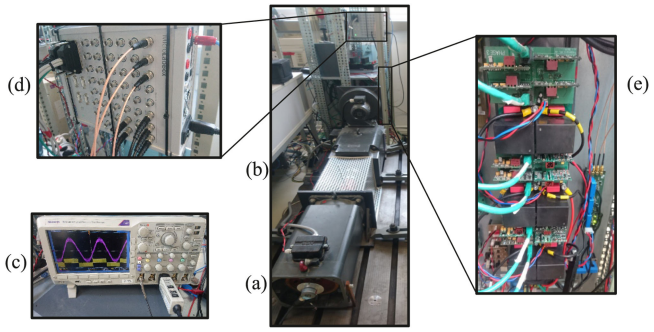

FIGURE 10. Experimental setup: (a) Siemens PMSM, (b) DC Load machine, (c) Oscilloscope, (d) dSPACE MicroLabBox, (e) Converter.

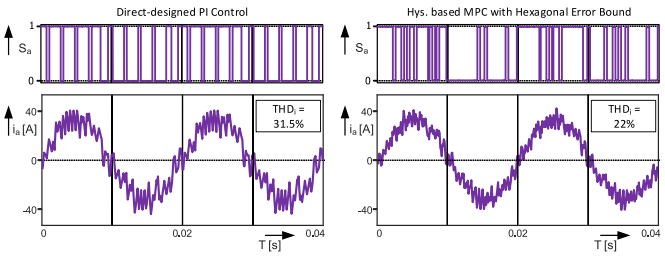

FIGURE 11. Comparison (laboratory) of VSI phase switching state and phase current of Direct-designed PI (left) and hys. based MPC with hexagonal Error Bound at $f_{sw(,eff)} = 1000$ Hz and $f_{el} = 50$ Hz.

and other disturbances, the predictions can be distorted and worsens the current distortion for all strategies.

Fig. 11 shows a comparison of the laboratory phase switching states and phase currents taken with the dSPACE ControlDesk. The direct-designed PI Control (left) is compared with the MPC with hexagonal current error shape (right). The machine is run at the same operation point of $f_{el} = 50$ Hz with an (effective) switching frequency of $f_{sw(,eff)} = 1000$ Hz. As it can be seen, the switching pattern of the direct-designed PI Control is evenly distributed, while the MPC has no regular pattern. The MPC algorithms only switches if necessary. This way, for the same effective switching frequency, the current harmonic can be reduced from $THD_i = 31.5\%$ with the direct-designed PI Control to $THD_i = 22\%$ using MPC.

The solid lines in Figure 12 show the measured results of the current distortion for different effective switching frequencies. The laboratory results prove the simulations. The deviations are very small, but increasing slightly at low carrier ratios.

In Fig. 13 the experimental results for the VR based active damping strategy is proven. While the inverter phase current (blue) is similar for both operation points, the filter voltage (green) and motor currents (teal) are highly distorted without active damping.

Figure 14 (solid lines) shows the experimental results for the 2-Level 3-phase VSI with sinewave filter. Due to the regular pattern of PWM based control, the direct designed

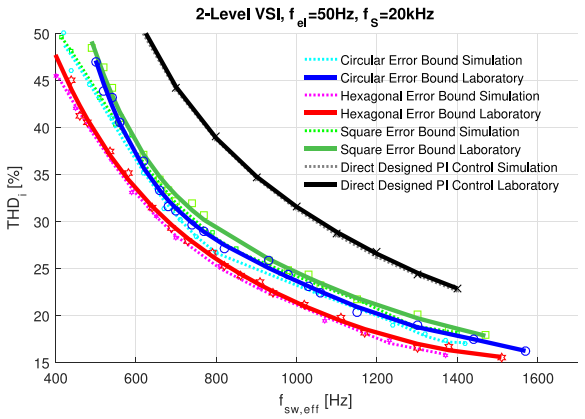

FIGURE 12. Comparison of simulation and experimental results for VSI, (eff.) switching frequency $f_{sw,eff}$ over total harmonic current distortion $\mathbf{THD_i}$ with constant el. frequency f_{el}.

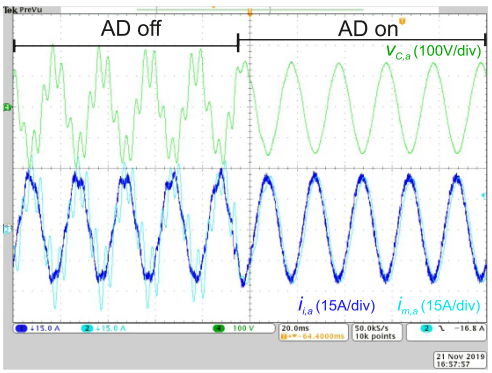

FIGURE 13. Experimental results for inverter phase current $i_{i,a}$ (blue), filter capacitor voltage $v_{C,a}$ (green), and motor phase current $i_{m,a}$ (teal), with and without Virtual Resistor (VR) based active damping (AD).

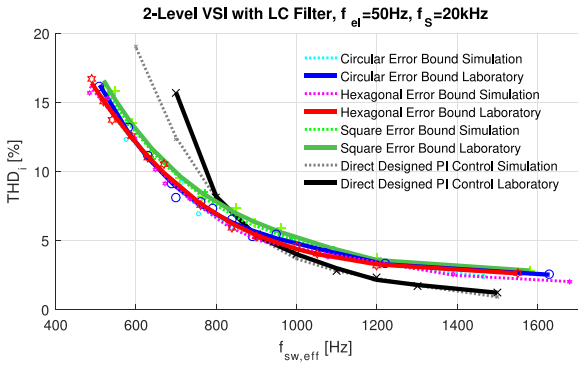

FIGURE 14. Comparison of simulation and experimental results for VSI with LC filter, (eff.) switching frequency $f_{sw,eff}$ over total harmonic current distortion $\mathbf{THD_i}$ with constant el. frequency f_{el}.

PI Control is providing the lowest current distortion at higher switching frequencies. The MPC based strategies would need a higher control frequency to reduce the THDi further. At switching frequencies below $f_{sw} \approx 900$ Hz , which is equal to a pulse ratio of 18, the predictive control is providing lower current distortion for the same switching frequencies.

Analogous to the case without motor filter, the hexagonal current error shape can be used to achieve the lowest current distortion.

VII. CONCLUSION

In this paper, the performance of hysteresis-based Model Predictive Control with MPC and sinewave filter is proven. Virtual resistor based active damping in combination with a Luenberger observer is used to guarantee stability. Different current error shapes for the 2-level 3-phase inverter are investigated. The hexagonal error shape provides the lowest current distortion compared to circular and square error bounds. Compared to a direct designed PI Control with PWM, without motor filter the effective switching frequency can be reduced by 25% and more. Adding the LC filter, the harmonic distortion can be improved effectively. While at high pulse ratios, the direct designed PI Control provides the lowest current distortion due to the regular switching pattern, for decreasing pulse ratios, predictive control algorithms can significantly improve the THDi and can be used to reduce the filter size.

REFERENCES

[1] Z. Mynar, L. Vesely, and P. Vaclavek, "PMSM model predictive control with field-weakening implementation," *IEEE Trans. Ind. Electron.*, vol. 63, no. 8, pp. 5156–5166, Aug. 2016.

[2] T. Baumgartner, R. M. Burkart, and J. W. Kolar, "Analysis and design of a 300-w 500000-r/min slotless self-bearing permanent-magnet motor," *IEEE Trans. Ind. Electron.*, vol. 61, no. 8, pp. 4326–4336, Aug. 2014.

[3] H. Abu-Rub, J. Holtz, J. Rodriguez, and G. Baoming, "Medium-voltage multilevel converters—state of the art, challenges, and requirements in industrial applications," *IEEE Trans. Ind. Electron.*, vol. 57, no. 8, pp. 2581–2596, Aug. 2010.

[4] S. Kouro, J. Rodriguez, B. Wu, S. Bernet, and M. Perez, "Powering the future of industry: High-power adjustable speed drive topologies," *IEEE Ind. Appl. Mag.*, vol. 18, no. 4, pp. 26–39, Jul. 2012.

[5] V. Blasko and V. Kaura, "A novel control to actively damp resonance in input LC filter of a three-phase voltage source converter," *IEEE Trans. Ind. Appl.*, vol. 33, no. 2, pp. 542–550, Mar./Apr. 1997.

[6] F. Morel, X. Lin-Shi, J.-M. Retif, B. Allard, and C. Buttay, "A comparative study of predictive current control schemes for a permanent-magnet synchronous machine drive," *IEEE Trans. Ind. Electron.*, vol. 56, no. 7, pp. 2715–2728, Jul. 2009.

[7] H. A. Young, M. A. Perez, and J. Rodriguez, "Analysis of finite-control-set model predictive current control with model parameter mismatch in a three-phase inverter," *IEEE Trans. Ind. Electron.*, vol. 63, no. 5, pp. 3100–3107, May 2016.

[8] Y. Wang *et al.*, "Deadbeat model-predictive torque control with discrete space-vector modulation for PMSM drives," *IEEE Trans. Ind. Electron.*, vol. 64, no. 5, pp. 3537–3547, May 2017.

[9] P. Kakosimos and H. Abu-Rub, "Deadbeat predictive control for PMSM drives with 3-l NPC inverter accounting for saturation effects," *IEEE J. Emerg. Sel. Topics Power Electron.*, vol. 6, no. 4, pp. 1671–1680, Dec. 2018.

[10] S. Walz, R. Lazar, G. Buticchi, and M. Liserre, "Dahlin-based fast and robust current control of a PMSM in case of low carrier ratio," *IEEE Access*, vol. 7, pp. 102 199–102 208, 2019.

[11] W. Xie *et al.*, "Finite-control-set model predictive torque control with a deadbeat solution for PMSM drives," *IEEE Trans. Ind. Electron.*, vol. 62, no. 9, pp. 5402–5410, Sep. 2015.

[12] J. Holtz, "Advanced PWM and predictive control—an overview," *IEEE Trans. Ind. Electron.*, vol. 63, no. 6, pp. 3837–3844, Jun. 2016.

[13] J. Scoltock, T. Geyer, and U. K. Madawala, "A comparison of model predictive control schemes for MV induction motor drives," *IEEE Trans. Ind. Informat.*, vol. 9, no. 2, pp. 909–919, May 2013.

[14] T. Barisa, S. Iles, D. Sumina, and J. Matusko, "Model predictive direct current control of a permanent magnet synchronous generator based on flexible Lyapunov function considering converter dead time," *IEEE Trans. Ind. Appl.*, vol. 54, no. 3, pp. 2899–2912, May 2018.

[15] X. Zhang, L. Zhang, and Y. Zhang, "Model predictive current control for PMSM drives with parameter robustness improvement," *IEEE Trans. Power Electron.*, vol. 34, no. 2, pp. 1645–1657, Feb. 2019.

[16] T. Geyer, "Model predictive direct current control: Formulation of the stator current bounds and the concept of the switching horizon," *IEEE Ind. Appl. Mag.*, vol. 18, no. 2, pp. 47–59, Mar. 2012.

[17] S. Walz, R. Lazar, and M. Liserre, "Multi-step model predictive control for a high-speed medium-power PMSM," in *Proc. IEEE Energy Convers. Congr. Expo.*, Sep. 2018, pp. 5040–5046.

[18] X. Zhang, Y. Wang, C. Yu, L. Guo, and R. Cao, "Hysteresis model predictive control for high-power grid-connected inverters with output LCL filter," *IEEE Trans. Ind. Electron.*, vol. 63, no. 1, pp. 246–256, Jan. 2016.

[19] J. Scoltock, T. Geyer, and U. K. Madawala, "A model predictive direct current control strategy with predictive references for MV grid-connected converters with LCL-filters," *IEEE Trans. Power Electron.*, vol. 30, no. 10, pp. 5926–5937, Oct. 2015.

[20] N. Panten, N. Hoffmann, and F. W. Fuchs, "Finite control set model predictive current control for grid-connected voltage-source converters with LCL filters: A study based on different state feedbacks," *IEEE Trans. Power Electron.*, vol. 31, no. 7, pp. 5189–5200, Jul. 2016.

[21] P. Falkowski and A. Sikorski, "Finite control set model predictive control for grid-connected AC–DC converters with LCL filter," *IEEE Trans. Ind. Electron.*, vol. 65, no. 4, pp. 2844–2852, Apr. 2018.

[22] J. Salomki and J. Luomi, "Vector control of an induction motor fed by a PWM inverter with output LC filter," *EPE J.*, vol. 16, no. 1, pp. 37–43, Feb. 2006.

[23] S. Mastellone, G. Papafotiou, and E. Liakos, "Model predictive direct torque control for MV drives with LC filters," in *Proc. 13th Eur. Conf. Power Electron. Appl.*, 2009.

[24] H. Kim, M. W. Degner, J. M. Guerrero, F. Briz, and R. D. Lorenz, "Discrete-time current regulator design for AC machine drives," *IEEE Trans. Ind. Appl.*, vol. 46, no. 4, pp. 1425–1435, Jul. 2010.

[25] S. Bolognani, S. Bolognani, L. Peretti, and M. Zigliotto, "Design and implementation of model predictive control for electrical motor drives," *IEEE Trans. Ind. Electron.*, vol. 56, no. 6, pp. 1925–1936, Jun. 2009.

[26] J. Lunze, *Regelungstechnik 2*. Berlin, Germany: Springer, 2016.